

EXTINCTIONS AND DISTANCES OF DARK CLOUDS FROM UGRIJHK PHOTOMETRY OF RED CLUMP GIANTS: THE NORTH AMERICA AND PELICAN NEBULAE COMPLEX

V. Straizys and V. Laugalys

*Institute of Theoretical Physics and Astronomy, Vilnius University,
Goštauto 12, Vilnius LT-01108, Lithuania; straizys@itpa.lt*

Received 2009 August 15; accepted 2009 August 28

Abstract. A possibility of applying 2MASS J , H , K_s , IPHAS r , i and MegaCam u , g photometry of red giants for determining distances to dark clouds is investigated. Red clump giants with a small admixture of G5–K1 and M2–M3 stars of the giant branch can be isolated and used in determining distances to separate clouds or spiral arms. Interstellar extinctions of background red giants can be also used for mapping dust surface density in the cloud.

Key words: ISM: dust clouds: individual (LDN 935) – stars: fundamental parameters (classification, colors) – photometric systems: 2MASS, IPHAS, MegaCam, Vilnius

1. INTRODUCTION

The determination of distances to dust and molecular clouds still remains a problem. One of the most popular methods in use is based on the extinction vs. distance plot – at the cloud distance, a steep rise in extinction takes place. The input observational data on stars, necessary for applying the method, are the apparent magnitudes and color indices (usually V and $B-V$), and two-dimensional spectral types (usually in the MK system) which are used to estimate of intrinsic color indices and absolute magnitudes. Magnitudes and color indices can be taken from observations in any photometric system, for example, in the system of the near infrared 2MASS survey (K_s magnitudes and $H-K_s$ color indices). Two-dimensional spectral types of stars can be determined either by classification of their spectra or by applying interstellar reddening-free quantities in one of multicolor photometric systems, for example, in the seven-color *Vilnius* photometric system.

The estimation of absolute magnitudes is the weakest point of the method. The absolute errors of M_V estimated from MK spectra can be as large as ± 0.5 mag, and this leads to the distance errors from -20% to $+26\%$. For supergiants, the absolute error of M_V can reach even ± 1.0 mag. Therefore, for more accurate distance determination a statistically significant number of stars is essential.

In the case of clouds located at distances > 1 kpc, two-dimensional classification of stars is complicated due to faintness of field stars, located at the cloud distance

or in its background, especially in the blue spectral range. Multicolor photometric systems, such as the *Vilnius* system (Straizys 1992), provide a means to classify stars using the interstellar reddening-free Q parameters, and they are able to reach much fainter and more distant stars than in the case of spectral classification. However, their usefulness declines when heavy interstellar extinction is present.

In such a case, near-infrared photometry is more favorable. 2MASS photometry in the J , H and K_s passbands (at 1.24, 1.66 and 2.16 μm) provides an effective tool for penetrating to distant sites of the Galaxy, hidden behind dense dust clouds. However, in the case of heavy and variable interstellar reddening, two-dimensional classification of stars using the infrared colors becomes impossible. For example, the sequences of stars of different luminosities in the two-color diagram $J-H$ vs. $H-K_s$ overlap even in the absence of interstellar reddening. The shift of stars along reddening lines complicates the situation even more.

Fortunately, in some of the cases, even near infrared photometry may be helpful. With a certain degree of confidence the use of interstellar reddening-free parameters Q_{JHK} enables us to identify K-type giants, AGB stars, OB stars and young stellar objects (YSOs) even at extremely large interstellar reddening (see Comeron & Pasquali 2005; Straizys & Laugalys 2007, 2008a,b,c, Straizys et al. 2008). Since this identification is not always single-valued, color indices or magnitudes, measured in other photometric passbands, could give the missing information in some cases.

For the determination of extinction and distance from J , H , K_s photometry we need to have a type of stars which is easily recognizable in the presence of heavy and variable interstellar reddening as only in such case one can estimate intrinsic colors and absolute magnitudes of individual stars. Such stars, shown to be extremely useful for the extinction investigation up to great distances, are red clump giants (hereafter RCGs) – stars in the post-helium-flash evolutionary stage, analogues of horizontal-branch stars of Population II. According to our previous investigation (Straizys & Lazauskaitė 2009), their mean intrinsic color indices are: $J-H = 0.46$ and $H-K_s = 0.09$.

Although spectral types of RCG stars are in the range from G8 III to K2 III, their absolute magnitudes in the K_s passband, M_{K_s} , show a surprising uniformity. Using the *Hipparcos* parallaxes, Alves (2000) has found that RCGs show a very small dispersion of absolute magnitudes in the K passband, $M_K = -1.61 \pm 0.03$ mag, without dependence on small differences in the temperature and metallicity. Later on, a similar conclusion was reached by Grocholski & Sarajedini (2002) who obtained for RCGs in open clusters $M_K = -1.62 \pm 0.21$ mag. These stars would be perfect distance and reddening indicators if we were able to identify them among thousands of stars with various spectral types and reddenings.

In the paper Straizys & Laugalys (2008c) we concluded that RCGs, intermingled with cooler stars of the giant sequence, are especially useful for the determination of slopes of interstellar reddening lines in the $J-H$ vs. $H-K_s$ diagram. In the present paper we investigate a possibility of isolating RCGs from other K–M III stars and using them for the cloud distance determination. We apply our method to the region near the Galactic plane, which includes the North America and Pelican nebulae (hereafter NAP) and the dark cloud between them. In this region, deep photometry is available in several broad-band systems: the 2MASS J,H,K_s system, the IPHAS r,i system and the MegaCam u,g system.

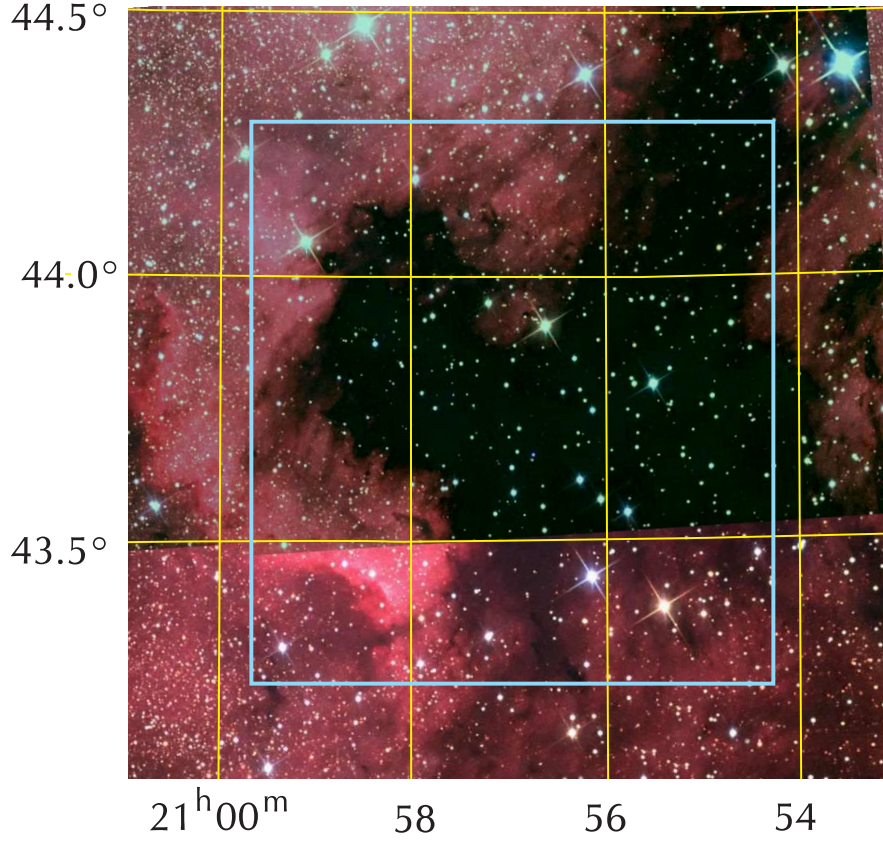


Fig. 1. The investigated area in the North America and Pelican nebulae complex (within the blue square).

2. THE AREA IN CYGNUS

The selected $1^\circ \times 1^\circ$ area in the NAP complex with the center at RA (J2000) = 20h57m, DEC (J2000) = $+43^\circ 45'$ is shown in Figure 1. It covers the southern part of the dark cloud LDN 935 (Lynds 1962) = TGU 497 (Dobashi et al. 2005), including the Gulf of Mexico, the ‘coastal’ areas around the Gulf, the Florida peninsula and the dark cloud up to the Pelican beak. The choice of this area was predetermined by the availability in it of deep photometry in the u and g passbands, obtained with the MegaCam mosaic CCD camera on CFHT (Gwyn 2008; MegaPipe 2009). The u and g filters of the MegaCam are similar, but not identical, to the Sloan Digital Sky Survey (SDSS) filters. The SDSS filter u has a ‘red leak’ at 710 nm, which precludes from applying the $u-g$ index for intrinsically red and heavily reddened stars (Covey et al. 2007). In the u filter of MegaCam the red leak is absent. The limiting u magnitude of the MegaCam catalog with an accuracy of < 0.1 mag is about 22.5.

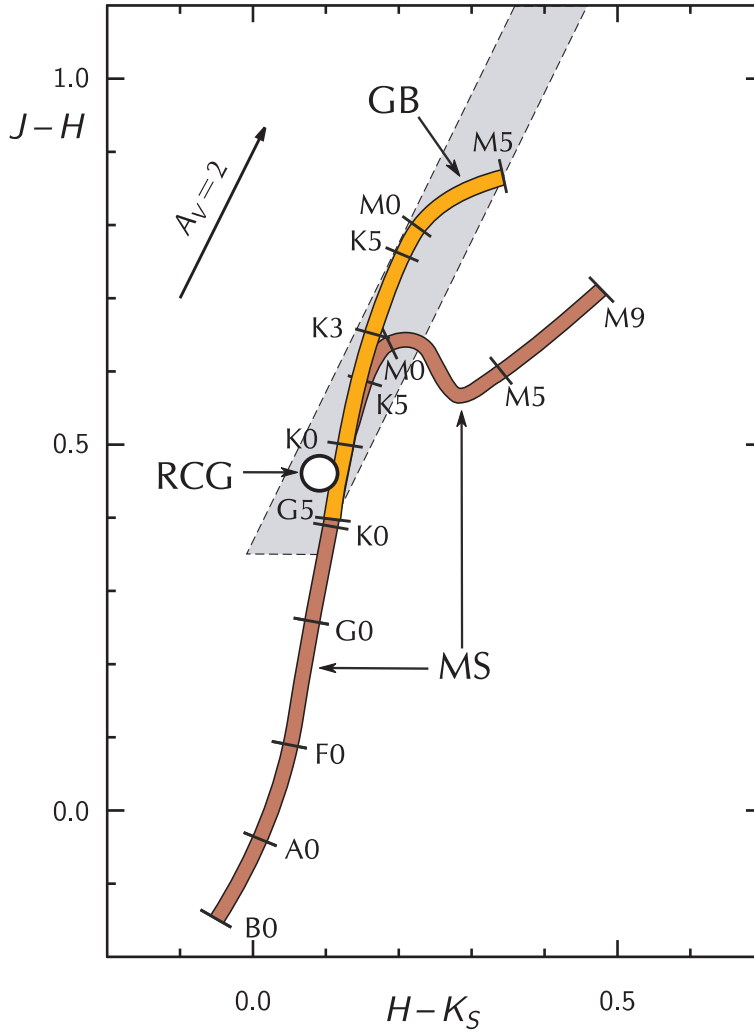


Fig. 2. The $J-H$ vs. $H-K_s$ diagram with the intrinsic main sequence (MS, brown belt), giant branch (GB, orange belt) and the locus of red clump giants (RCG, white circle). Two parallel broken lines mark the region in which RCGs with different interstellar reddenings are located (grey strip). The length of the reddening vector corresponds to $A_V = 2$ mag.

The r and i magnitudes were taken from the INT Photometric $H\alpha$ Survey (IPHAS) since the original SDSS photometry in the whole area is not available. This survey covers the northern Milky Way between Galactic longitudes $30-220^\circ$ and latitudes $\pm 5^\circ$ (Drew et al. 2005). The objects are measured in two broad-band filters, r' and i' , and one narrow-band filter placed on $H\alpha$. The r' and i' filters are similar to those of the SDSS u', g', r', i', z' system, their mean wavelengths are at 624 nm and 774 nm. For simplicity, in this paper we will omit the ‘prime’ designations of the IPHAS magnitudes.

To define the identification criteria of RCG stars we investigated their location

in the $J-H$ vs. $H-K_s$ and $u-g$ vs. $r-i$ diagrams with respect to the sequences of luminosity V and III stars (main-sequence stars and giants) in the presence of considerable and variable interstellar reddening.

3. RED CLUMP GIANTS IN THE $J-H$, $H-K_s$ DIAGRAM

Figure 2 shows the intrinsic sequences of luminosity V and III stars in the 2MASS $J-H$ vs. $H-K_s$ diagram according to Straizys & Lazauskaitė (2009). The sequence of unreddened main-sequence stars of spectral classes from A to M has been determined using field stars up to 40 pc from the Sun with available MK spectral types and stars of the Praesepe, Pleiades and M 39 open clusters with small dereddening corrections. Intrinsic colors of O and B stars have been determined by dereddening the corresponding stars in the Ori OB1 association, the Collinder 121 and the Pleiades clusters and field O-type stars with low reddenings. For determining the intrinsic colors of G5–M5 III stars, dereddened giants from seven open clusters and field giants from the NGP region have been used. The approximate color indices of RCGs in the diagram have been estimated by locating the center of the apparent crowding of dereddened positions of the cluster giants.

It is evident that the $J-H$ vs. $H-K_s$ diagram does not allow us to isolate RCGs in the presence of interstellar reddening since their reddening line runs approximately along the sequences of dwarfs and giants. Taking into account that the scattering of color indices $H-K_s$ due to intrinsic dispersion and observational errors is about ± 0.05 mag (see Straizys & Lazauskaitė 2009), the strip of reddened RCGs (shown in Figure 1 in grey) is drawn with a 0.2 mag width (in $H-K_s$). It covers the main sequence in the G2–M2 range and the giant branch in the G5–M5 range. Luminosity class IV stars (subgiants) of spectral types G5–K2 IV should also fall within the same strip.

Since G5–M dwarfs are absolutely faint, they are not seen at large distances. Contamination of the RCG strip from such stars can be eliminated easily by setting an apparent magnitude limit in the K_s vs. $H-K_s$ (magnitude-color) diagram.

However, contamination of the RCG strip by cooler giants is a serious problem. The giant sequence stars from K3 III to M5 III have more negative M_{K_s} magnitudes than RCGs, thus they are apparently brighter and are visible at larger distances. Although the space density of RCGs outnumbers considerably that of K3–M5 III stars (Perryman et al. 1995, 1997; Alves 2000), the surface density of the latter is quite high. Also, in the $J-H$ vs. $H-K_s$ diagram the RCGs are mixed with giants of spectral types G5–K2 III which in the HR diagram are on the ascending giant branch, i.e., burning hydrogen in a shell around the helium core. However, their luminosities in the K_s passband do not differ considerably from those of RCGs, and their presence in the sample does not distort the dependence of the extinction on distance. Hereafter, for simplicity, we will call all these stars as RCGs.

Consequently, the main problem is the isolation of RCGs (together with the intervening G5–K2 giants of the ascending branch) from cooler stars of the red giant sequence, since J , H , K photometry alone cannot help much. We have to address the passbands of other photometric systems. Since we are usually dealing with faint stars, broad-band systems are preferable.

4. SYNTHETIC COLORS IN THE u, g, r, i SYSTEM

For the separation of RCGs from cooler giants we have applied the $u-g$ vs. $r-i$ diagram where u and g are from the MegaCam and r and i are from the IPHAS surveys. Intrinsic color indices $u-g$ and $r-i$ for the main-sequence stars, red giants and F–G–K subdwarfs were calculated by the equation:

$$m_1 - m_2 = -2.5 \log \frac{\int F(\lambda) \tau^x(\lambda) R_1(\lambda) d\lambda}{\int F(\lambda) \tau^x(\lambda) R_2(\lambda) d\lambda} + \text{const}, \quad (1)$$

where $F(\lambda)$ are the flux distribution functions of stars in energy units for the unit wavelength intervals, $\tau^x(\lambda)$ is the transmittance function of x units of interstellar dust (from Straižys 1992), $R_1(\lambda)$ and $R_2(\lambda)$ are the response-to-energy functions of passbands 1 and 2. The value of constant makes all color indices of A0 V star to be zeros. Spectral energy distributions for stars of luminosities V and III were taken from Sviderskienė (1988) and for F–G–K subdwarfs from Sviderskienė (1992).

Color indices can be used to calculate interstellar reddening-free Q -parameters:

$$Q_{1234} = (m_1 - m_2) - (E_{12}/E_{34})(m_3 - m_4), \quad (2)$$

here

$$E_{k,\ell} = (m_k - m_\ell)_{\text{reddened}} - (m_k - m_\ell)_{\text{intrinsic}}. \quad (3)$$

The response-to-energy functions, $R(\lambda)$, for the r and i filters in the IPHAS system were obtained by the equation:

$$R(\lambda) = \lambda f(\lambda) QE(\lambda), \quad (4)$$

where $f(\lambda)$ are relative filter transmittances and $QE(\lambda)$ is the quantum efficiency function of a CCD camera. The filter transmittance and the quantum efficiency functions were taken from the INT WFC and IPHAS Internet sites.¹ The response-to-energy functions of the MegaCam u and g magnitudes were obtained in a similar way, but the filter transmittances and the MegaCam quantum efficiency curve were taken from the MegaCam Internet site.²

Since the observed MegaCam u and g magnitudes are in the AB magnitude system³, and our synthetic color indices $u-g$ are normalized to zero for the A0 V star (Vega), we have corrected the synthetic indices by adding a constant of 0.438 mag. The $r-i$ synthetic color indices were used unchanged since the observed IPHAS r and i magnitudes use the Vega-based zero-point. The $g-r$ synthetic color indices have mixed zero-point systems – they were corrected by subtracting 0.09 mag. The values of the corrections were taken from the MegaCam Internet site. The accepted values of the intrinsic color indices $u-g$, $g-r$ and $r-i$ are listed in Table 1.

The slopes of reddening lines in the diagram $u-g$ vs. $r-i$ depend slightly on spectral type. For early K-giants the ratio E_{u-g}/E_{r-i} is ~ 1.50 , for late K- and early M-giants it is ~ 1.45 . The ratios E_{g-r}/E_{r-i} are 1.40 and 1.35, respectively.

The schematic $u-g$ vs. $r-i$ diagram is shown in Figure 3. The sequences for M-type stars of luminosity V and III classes are slightly smoothed. The exact

¹ <http://www.iphas.org> and <http://www.ing.iac.es/Astronomy/instruments/wfc>

² <http://www2.cadc-ccda.hia-ihp.nrc-cnrc.gc.ca/megapipe/docs/filters.html>

³ For the definition of the system see Oke (1965), AB means ‘ABsolute’ flux.

Table 1. The synthetic intrinsic color indices $u-g$, $g-r$ and $r-i$ accepted for luminosity V and III stars and F–G subdwarfs. Zero-points of color indices $u-g$ are in the MegaCam AB system, of $r-i$ in the IPHAS Vega system and of $g-r$ in the mixed system (see the text).

MK type	$u-g$	$g-r$	$r-i$	MK type	$u-g$	$g-r$	$r-i$
B0 V	−0.33	−0.35	−0.15	G5 III	1.37	0.73	0.45
A0 V	0.44	−0.09	0.00	G8 III	1.53	0.79	0.47
F0 V	0.70	0.22	0.20	K0 III	1.69	0.85	0.50
G0 V	0.94	0.48	0.36	K1 III	1.82	0.92	0.54
K0 V	1.32	0.71	0.43	K2 III	1.99	1.00	0.57
K2 V	1.48	0.79	0.48	K3 III	2.28	1.07	0.58
K3 V	1.66	0.89	0.54	K4 III	2.42	1.20	0.67
K5 V	1.98	1.15	0.66	K5 III	2.61	1.31	0.80
M0 V	2.16	1.36	0.90	M0 III	2.73	1.33	0.90
M2 V	2.24	1.43	1.16	M2 III	2.76	1.39	1.06
M4 V	2.11	1.48	1.53	M3 III	2.70	1.42	1.29
M5 V	2.31	1.52	1.69	M4 III	2.55	1.43	1.62
M7 V	2.42	1.63	2.06	M5 III	2.35	1.51	1.96
sd FG	0.60	0.41	0.35	M6 III	2.05	1.65	2.32

position of RCGs in the diagram is unknown. On the analogy with the $J-H$ vs. $H-K_s$ diagram, their locus was taken on the giant branch (GB), corresponding to spectral type G8 III. The center line of the grey strip corresponds to

$$Q_{ugri} = (u - g) - 1.50 (r - i) = 0.83, \quad (5)$$

the boundary values are 0.68 and 0.98. We accept that with the increase of interstellar reddening RCGs move upward and right along this strip. The strip extends over the main-sequence stars of spectral classes K0–M1 and crosses the giant branch at \sim M3 III. This means that this diagram alone cannot isolate RCGs and intervening stars of spectral classes G5–K1 of the giant sequence.

In an attempt to identify RCGs, we decided to combine the $J-H$ vs. $H-K_s$ (Figure 2) and $u-g$ vs. $r-i$ (Figure 3) diagrams. But first we have to identify the main features seen in the observed diagrams of the NAP field.

5. THE OBSERVED $u-g$, $r-i$ DIAGRAM

In the NAP field shown in Figure 1 we identified about 2500 stars having measurements in the MegaCam u and g , the IPHAS r and i and the 2MASS J , H , K_s magnitudes. The magnitudes u , g , r , i were taken up to an accuracy of 0.1 mag, while for the 2MASS magnitudes the accuracy limit was 0.05 mag. Figure 4 shows the $u-g$ vs. $r-i$ diagram for the selected sample together with the sequences of luminosity V and III stars and the interstellar reddening vector.

The distribution of stars in this diagram is the combined result of real distribution of stars on the intrinsic sequences of different luminosity classes, different shifts of stars along their reddening lines, and the limiting magnitudes both at the bright and faint ends of different passbands. Limiting magnitudes depend not only on the exposure lengths but also on the temperature, luminosity and interstellar reddening. At the faint end the limiting magnitude is defined mainly by the signal-to-noise (S/N) ratio and the accepted accuracy limit, at the bright end it is defined by the saturation of images in CCD detectors. Among the four passbands

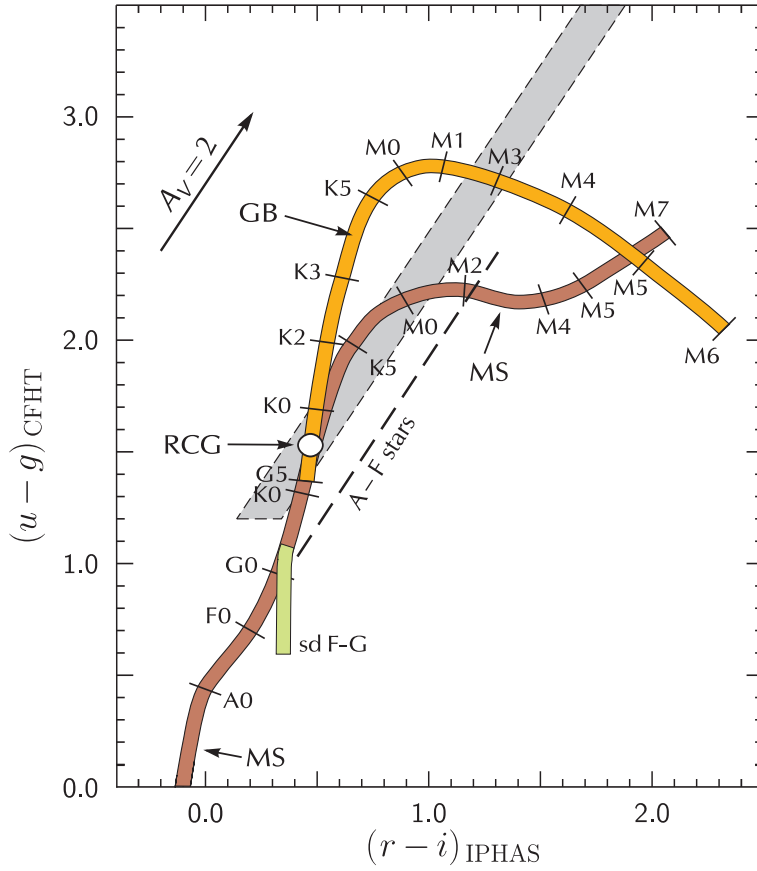


Fig. 3. The $u-g$ vs. $r-i$ diagram with the intrinsic main sequence (MS, brown belt), the giant branch (GB, orange belt), the locus of red clump giants (RCG, white circle) and the sequence of F-G subdwarfs (sd F-G, green strip). Two parallel broken lines mark the boundaries of the grey strip in which RCGs with different interstellar reddenings should be located. The length of the reddening vector corresponds to $A_V = 2$ mag.

used (Figure 4) the worst S/N ratio is for the u magnitude since in the ultraviolet the CCD+filter sensitivity is the lowest and in this spectral region cool and heavily reddened stars (which are the objects of our interest) are quite faint.

Figure 5 shows the distribution of stars in our sample with respect to magnitude in the four passbands. The faintest limiting magnitudes are close to $u = 22$, $g = 20$, $r = 18$ and $i = 16.5$. The brightest end for u and g magnitudes is close to 13 and for r and i close to 12. This means that in our sample all stars brighter than $r = 12$ are missing, and this magnitude cut eliminates from the sample some types of stars at small distances from the Sun, such as B, A and F stars up to a few hundreds of parsecs.

At first glance, we can spot in the $u-g$ vs. $r-i$ diagram some outstanding features. First, we see a well populated intrinsic sequence of G, K and early M dwarfs. The coolest dwarfs are absolutely faint, especially in the ultraviolet, and they are rare in the selected sample. The stars of spectral classes B, A and F are absent on

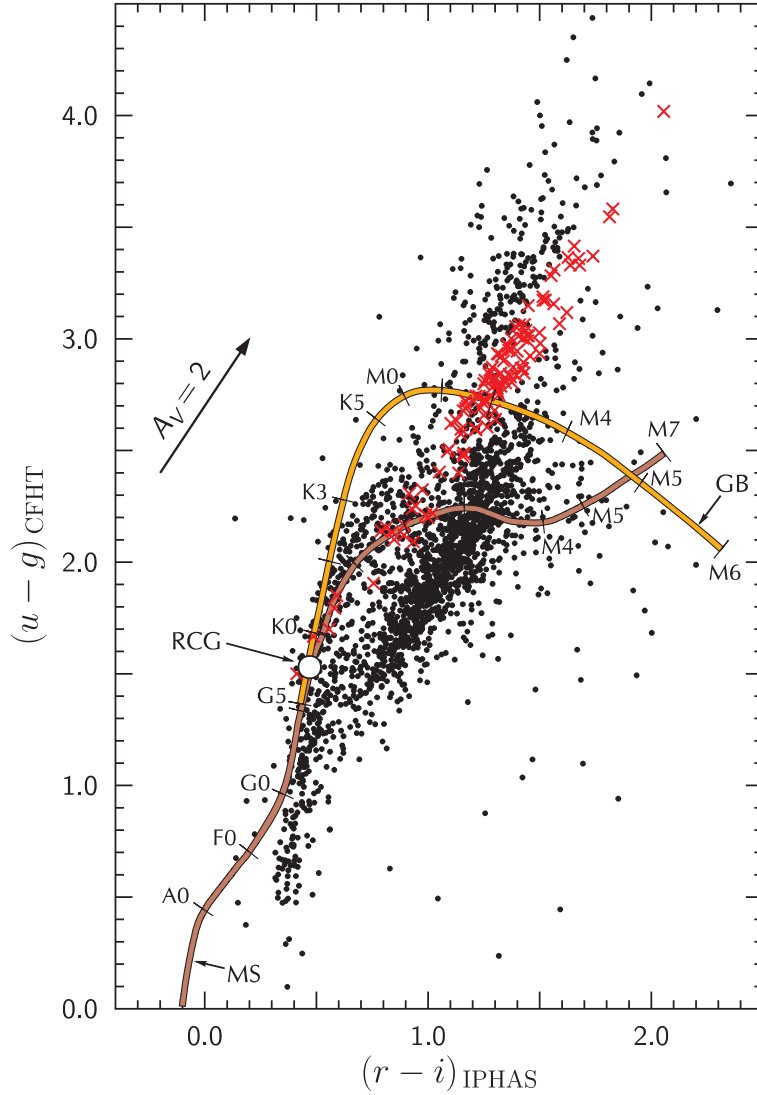


Fig. 4. Observed stars in the $u-g$ vs. $r-i$ diagram. The main sequence, giant branch and the locus of red clump giants are overplotted from Figure 3. Red crosses denote the suspected RCGs (see the text).

the intrinsic main sequence since they are too bright in u and g . The stars of latest B subclasses and of all A subclasses form a rich-populated sequence with different reddenings which extends from $r-i = 0.4$ to 1.5 or even farther to the red. Due to their high luminosity and relatively high space density these stars are seen at large distances. Except for A-type stars, whose intrinsic sequence runs almost along the reddening line, the sequence of reddened stars should also contain F-type stars, but due to their lower luminosity they are expected to be numerous only at small distances and reddenings.

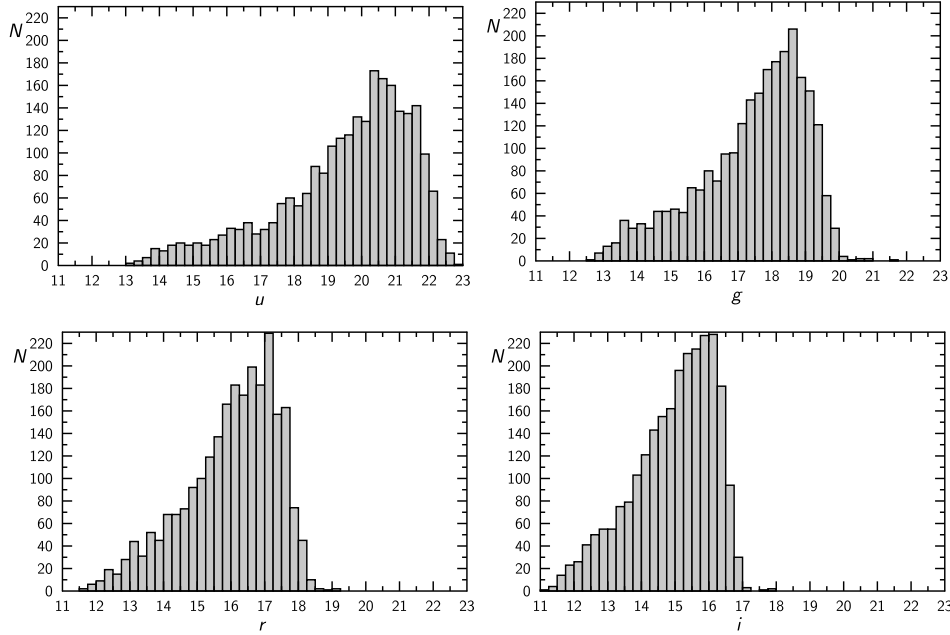


Fig. 5. Distributions by magnitudes u , g , r and i of the 2500 stars in the selected sample.

The second rich sequence, running more or less in parallel with the sequence of A stars and lying above it, corresponds to K–M giants, including RCGs – it extends from $r-i = 0.5$ to ~ 2.0 . This sequence is broader since the intrinsic line of red giants runs at a considerable angle with respect to the direction of reddening lines. The sequence includes a sample of stars shown as red crosses. At present it is sufficient to say that these stars are supposed RCGs. For the procedure of their identification see Section 7.

The next feature seen in the $u-g$ vs. $r-i$ diagram is the strip of possible F–G metal-deficient dwarfs (subdwarfs) at $r-i = 0.35$. Most of them should be located in front of the NAP complex and therefore have low reddenings. In the same region of the diagram and farther to the right we could find also reddened B-type stars of early subclasses, if such were present in the sample. However, it is easy to separate reddened B stars from unreddened F–G subdwarfs in the $J-H$ vs. $H-K_s$ diagram. None star located in this strip has been found to be a reddened B star.

6. THE OBSERVED $J-H$ vs. $H-K_s$ DIAGRAM

The $J-H$ vs. $H-K_s$ diagram for the same list of stars is plotted in Figure 6. The stars lower than $J-H < 0.2$ are absent due to the saturation effect in the u and partly g images of the MegaCam system. At larger values of $J-H$ crowding of stars and overlapping of the reddened sequences is much larger than it was observed in the $u-g$ vs. $r-i$ diagram. Comparing Figures 6 and 2, we can identify some of the features seen in the $u-g$ vs. $r-i$ diagram. The sequence of unreddened G dwarfs is seen only from $J-H = 0.25$ to 0.4 (G0–K0 V). K- and M-dwarfs are completely overlapped with giants. The largest concentration of reddened A stars is moved

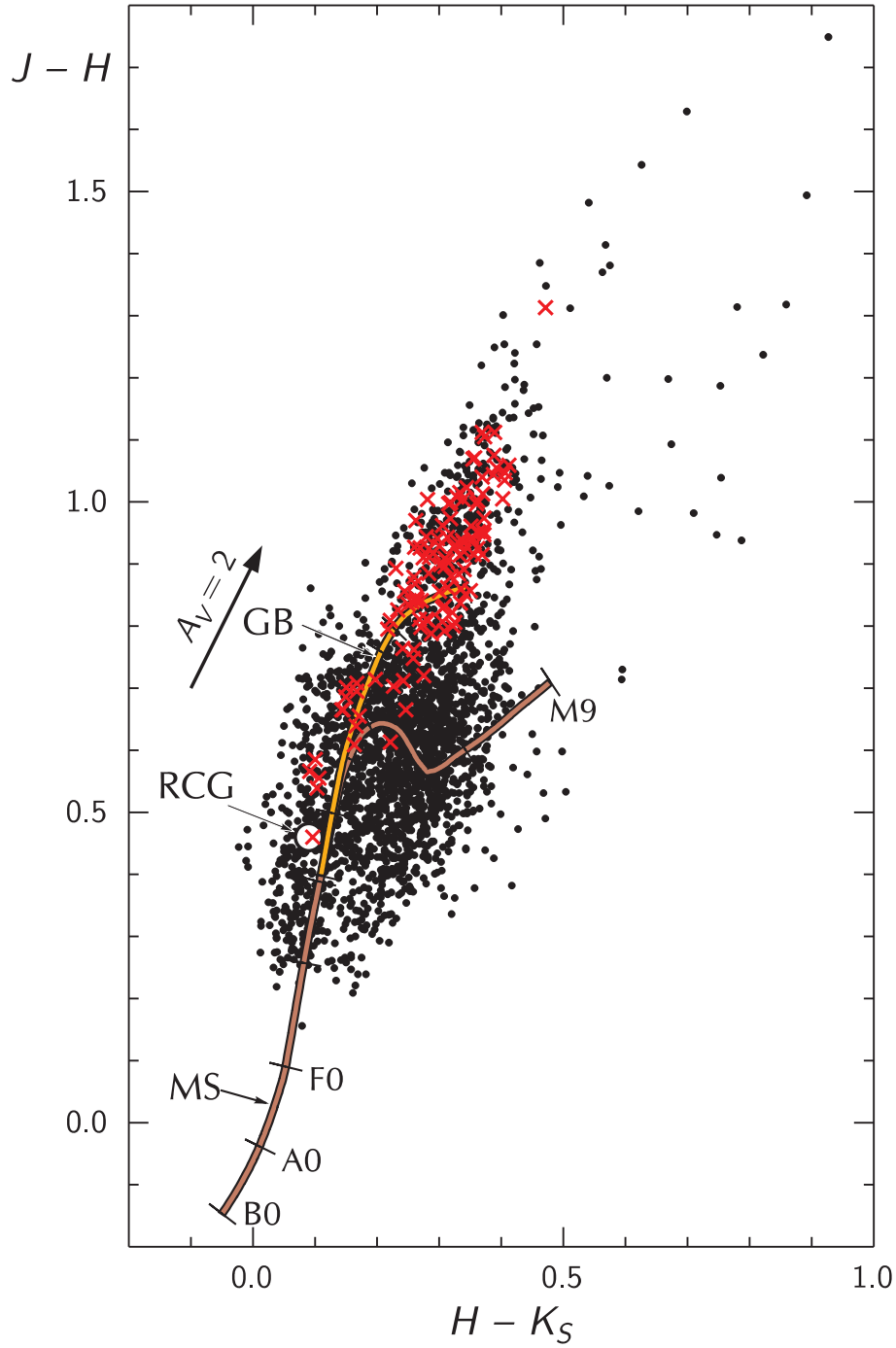


Fig. 6. Observed stars in the $J-H$ vs. $H-K_s$ diagram. The main sequence, giant branch and the locus of red clump giants are overplotted from Figure 2. Red crosses denote the suspected RCGs.

onto the M-dwarf sequence and to both sides of it. The sequence of reddened K–M giants is seen more distinctly, being narrower than in the $u-g$ vs. $r-i$ diagram. However, as it is evident from Figure 2, K and M giants of different reddenings, including RCGs (shown as red crosses), overlap each other.

In Figure 6 there are seen two groups of 44 dots deviating considerably to the right of the described sequences, and having Q_{JHK_s} between -0.2 and -0.8 . This is a typical domain of pre-main-sequence stars (PMSs or YSOs) where Herbig Ae/Be and T Tauri stars are located (see Figures 5 and 6 in Corbally et al. 2009). T Tauri stars can be present only in the upper group with $J-H > 0.9$ and $H-K_s > 0.6$. Two of them are known T Tauri stars, V 1539 Cyg and V 521 Cyg. The lower group of points probably contains massive YSOs of Herbig Ae/Be type. Some heavily reddened Herbig stars can be also present in the upper group. However, we do not exclude the possibility that some of these objects can be AGB stars, point-like galaxies or quasars.

7. ISOLATION OF RED CLUMP GIANTS

For the isolation of RCGs (together with G5–K1 giants on the ascending branch), we adopted several conditions ensuring the exclusion of overlapping stars from other sequences.

1. In the $J-H$ vs. $H-K_s$ diagram the requirement was set that the star must lie inside the grey strip shown in Figure 2, outlined by the reddening lines with Q_{JHK_s} between 0.18 and 0.38.

2. In the $u-g$ vs. $r-i$ diagram, the requirement was set that the star must lie inside the grey strip shown in Figure 3, outlined by the reddening lines with Q_{ugri} between 0.68 and 0.98. This requirement separates RCG stars from giants cooler than K1. Since the strip crosses the red giant sequence at class M3, it is impossible to separate reddened RCGs from stars of types M2–M3 III.

3. Again in the $J-H$ vs. $H-K_s$ diagram, in an attempt to exclude the main sequence stars earlier than $\sim K3 V$ and giants hotter than RCGs, we accepted the following two conditions: $J-H > 0.46$ and $H-K_s > 0.09$. These color cuts correspond to the intrinsic colors of RCGs, and they preclude the appearance between RCGs of stars with negative color excesses.

4. Even with these four conditions met, the selected RCG sample includes an admixture of the main-sequence stars – unreddened dwarfs of types K3–M1 V and reddened dwarfs of types K0–M1 V. To exclude most of them, we added one more condition, $K < 12 + 2.0(H-K_s)$, specific for the NAP region. This restriction cuts the red dwarfs of types G5 V and cooler, located at and beyond the distance of the NAP complex.

Applying these conditions, we have selected a sample of 104 stars, listed in Table 2, which are probable RCGs with an admixture of normal giant branch stars of spectral classes G5–K1 III and $\sim M3$ III. In Figures 4 and 6 these stars are plotted as red crosses. All these stars lie within the grey strips shown in Figures 2 and 3. However, within these strips we find also many unreddened and reddened main-sequence stars (and subgiants), mostly of spectral classes G8–K, which do not satisfy conditions (3) and (4).

Table 2. Stars in the NAP area with photometric properties of red clump giants in the 2MASS, IPHAS and MegaCam systems. 17 stars with the numbers flagged with asterisks probably have luminosities lower than those of RCGs. For these stars the extinction and distance values are not given.

No.	RA (2000)	DEC (2000)	K_s	$J-H$	$H-K_s$	$u-g$	$g-r$	$r-i$	A_V	d (kpc)
1*	313.566	43.729	11.022	0.555	0.106	1.793	1.156	0.582		
2*	313.583	43.438	11.664	0.639	0.166	2.101	1.306	0.848		
3	313.635	43.309	9.963	1.069	0.354	3.582	1.989	1.827	4.38	1.61
4*	313.661	43.564	11.674	0.539	0.103	1.700	1.000	0.557		
5	313.665	43.504	9.362	1.059	0.412	3.370	2.308	1.738	5.34	1.15
6	313.687	43.278	11.706	0.927	0.324	3.012	1.969	1.405	3.88	3.69
7	313.687	43.330	9.015	0.905	0.312	2.951	1.877	1.373	3.69	1.08
8*	313.693	44.233	11.682	0.609	0.163	1.906	1.038	0.756		
9	313.726	43.384	10.281	1.044	0.387	3.415	2.206	1.655	4.93	1.80
10*	313.734	43.339	12.148	0.626	0.149	2.009	1.138	0.732		
11*	313.791	43.379	11.278	0.695	0.167	2.165	1.263	0.894		
12	313.792	43.274	11.229	0.807	0.305	2.949	1.924	1.361	3.57	3.01
13*	313.830	44.241	10.694	0.665	0.143	2.155	1.226	0.813		
14	313.844	43.522	7.837	1.105	0.373	3.547	2.520	1.813	4.70	0.59
15	313.914	44.048	7.537	1.313	0.471	4.019	2.711	2.056	6.33	0.47
16*	313.934	44.240	12.266	0.632	0.160	2.083	1.129	0.769		
17	313.971	44.212	8.173	1.055	0.392	3.283	2.178	1.551	5.01	0.68
18	313.981	44.147	8.304	1.035	0.405	3.330	2.281	1.679	5.23	0.71
19*	314.007	44.021	9.891	0.665	0.145	2.141	1.298	0.790		
20	314.032	44.233	10.897	0.891	0.340	2.639	1.828	1.302	4.15	2.50
21	314.034	44.244	10.524	0.953	0.370	3.014	2.064	1.444	4.65	2.05
22	314.059	43.326	9.087	1.040	0.369	3.360	2.215	1.674	4.63	1.06
23	314.067	44.149	11.089	0.941	0.297	2.902	1.923	1.338	3.44	2.85
24	314.080	44.076	11.708	0.798	0.270	2.486	1.590	1.162	2.99	3.88
25	314.090	44.243	9.794	0.938	0.337	2.867	1.995	1.423	4.10	1.51
26	314.098	44.258	9.835	1.075	0.388	3.330	2.324	1.637	4.95	1.47
27	314.100	44.056	10.279	0.832	0.308	2.692	1.778	1.234	3.62	1.94
28	314.133	44.264	9.560	0.909	0.309	2.814	1.872	1.255	3.63	1.39
29	314.137	43.981	11.133	0.920	0.340	3.003	1.968	1.425	4.15	2.79
30	314.176	44.159	11.102	0.914	0.333	2.720	1.830	1.263	4.03	2.77
31*	314.215	43.714	12.048	0.619	0.165	1.901	1.043	0.713		
32*	314.216	43.387	11.538	0.714	0.197	2.121	1.076	0.892		
33	314.221	44.273	12.262	0.809	0.282	2.767	1.876	1.308	3.19	4.96
34	314.223	44.229	11.035	0.899	0.302	2.782	1.726	1.288	3.52	2.76
35	314.225	44.136	11.823	0.934	0.339	2.806	1.913	1.375	4.13	3.84
36*	314.243	43.300	11.285	0.708	0.167	2.220	1.324	1.019		
37	314.283	43.699	11.088	0.973	0.318	2.744	2.044	1.215	3.79	2.79
38	314.301	44.252	10.898	0.935	0.330	2.830	1.864	1.369	3.98	2.53
39	314.332	44.210	10.011	1.013	0.370	3.068	2.178	1.589	4.65	1.62
40	314.338	44.068	10.755	0.915	0.356	3.062	1.944	1.410	4.42	2.31
41	314.388	43.577	10.063	0.974	0.372	3.364	2.126	1.627	4.68	1.65
42	314.402	44.067	10.512	1.004	0.338	3.156	2.030	1.563	4.12	2.10
43	314.428	43.254	10.320	0.911	0.284	2.817	1.827	1.286	3.22	2.02
44*	314.443	43.305	9.409	0.655	0.171	2.136	1.451	0.839		

Table 2. Continued

No.	RA (2000)	DEC (2000)	K_s	$J-H$	$H-K_s$	$u-g$	$g-r$	$r-i$	A_V	d (kpc)
45	314.458	44.160	11.139	1.023	0.344	3.118	2.153	1.622	4.22	2.79
46	314.471	43.442	10.956	0.929	0.300	2.750	1.791	1.318	3.49	2.67
47	314.476	44.212	11.488	0.997	0.315	3.173	2.003	1.516	3.73	3.36
48	314.491	43.502	10.264	0.879	0.259	2.859	1.785	1.276	2.81	2.01
49	314.503	44.216	9.460	0.924	0.283	2.841	1.736	1.364	3.20	1.36
50	314.522	43.423	11.188	0.809	0.221	2.599	1.595	1.213	2.17	3.20
51	314.529	43.419	12.060	0.811	0.268	2.595	1.671	1.148	2.96	4.57
52	314.531	43.581	12.282	0.884	0.331	2.973	1.901	1.356	4.00	4.78
53	314.534	43.520	11.579	0.712	0.242	2.307	1.302	0.916	2.52	3.75
54	314.541	43.291	11.578	0.862	0.313	2.799	1.806	1.250	3.70	3.51
55	314.545	43.886	10.869	1.047	0.406	2.923	1.194	1.457	5.25	2.33
56	314.547	43.259	12.013	0.788	0.287	2.399	1.612	1.137	3.27	4.40
57	314.553	44.138	10.289	0.962	0.305	3.038	1.931	1.438	3.57	1.95
58	314.555	43.436	11.254	0.840	0.263	2.474	1.536	1.157	2.87	3.17
59	314.574	43.407	11.480	0.843	0.264	2.688	1.644	1.169	2.89	3.51
60	314.596	44.273	10.084	0.943	0.313	3.001	1.975	1.373	3.70	1.76
61*	314.598	43.555	12.243	0.515	0.146	1.608	0.830	0.533		
62	314.605	44.136	10.686	0.880	0.319	3.063	1.888	1.432	3.80	2.32
63	314.615	44.162	11.264	0.839	0.256	2.722	1.692	1.256	2.76	3.20
64	314.621	43.451	12.517	0.864	0.299	2.673	1.746	1.202	3.47	5.49
65	314.637	43.438	10.614	0.868	0.261	2.719	1.667	1.171	2.84	2.36
66	314.652	44.227	9.541	0.938	0.353	3.013	1.863	1.450	4.37	1.32
67*	314.665	44.018	11.857	0.460	0.096	1.500	0.700	0.412		
68	314.671	43.532	10.389	0.860	0.335	2.606	1.719	1.265	4.07	1.99
69	314.675	43.548	12.127	0.943	0.352	2.805	1.916	1.324	4.35	4.37
70	314.681	43.650	10.498	0.748	0.258	2.324	1.408	0.975	2.79	2.25
71*	314.687	44.134	12.135	0.499	0.135	1.672	0.725	0.549		
72	314.695	43.258	11.629	0.999	0.318	2.966	1.950	1.357	3.79	3.58
73	314.705	43.597	11.374	0.997	0.360	3.055	2.021	1.392	4.48	3.06
74	314.732	43.487	10.966	0.846	0.262	2.697	1.675	1.176	2.86	2.78
75	314.733	43.528	11.473	0.925	0.362	2.868	1.848	1.418	4.51	3.20
76	314.753	44.234	9.533	1.112	0.389	3.173	1.997	1.526	4.96	1.27
77	314.763	43.505	12.042	0.762	0.259	2.505	1.618	1.095	2.81	4.57
78*	314.773	43.665	12.237	0.621	0.155	1.853	1.071	0.647		
79	314.773	43.323	12.279	0.829	0.305	2.932	1.893	1.315	3.57	4.89
80	314.777	43.952	10.712	1.002	0.362	2.980	2.074	1.503	4.51	2.25
81	314.798	43.322	11.187	0.952	0.371	3.309	2.134	1.565	4.67	2.78
82	314.821	43.483	11.985	0.918	0.290	2.843	1.805	1.274	3.32	4.33
83	314.825	44.134	12.226	0.843	0.238	2.414	1.586	1.030	2.46	5.08
84	314.842	43.338	11.153	0.961	0.351	3.149	2.031	1.448	4.33	2.79
85	314.847	44.225	12.183	1.005	0.402	2.779	2.030	1.310	5.18	4.28
86	314.858	43.456	11.208	0.910	0.274	2.821	1.826	1.300	3.05	3.07
87	314.858	44.196	10.491	0.947	0.372	2.716	1.983	1.245	4.68	2.02
88	314.860	43.346	10.522	0.952	0.363	3.188	2.117	1.515	4.53	2.06
89	314.870	44.164	10.877	1.008	0.328	2.847	1.794	1.430	3.95	2.51
90	314.877	43.382	11.558	0.885	0.283	2.872	1.804	1.288	3.20	3.58
91	314.890	44.130	12.260	1.015	0.333	3.027	1.581	1.499	4.03	4.72

Table 2. Continued

No.	RA (2000)	DEC (2000)	K_s	$J-H$	$H-K_s$	$u-g$	$g-r$	$r-i$	A_V	d (kpc)
92	314.900	43.502	9.450	0.856	0.244	2.634	1.504	1.128	2.56	1.40
93	314.903	44.122	10.433	0.826	0.233	2.488	1.452	1.159	2.37	2.23
94	314.905	43.411	10.127	0.856	0.300	2.743	1.662	1.228	3.49	1.82
95	314.906	43.800	11.692	0.811	0.279	2.496	1.953	1.086	3.14	3.82
96	314.909	43.549	11.567	0.841	0.271	2.728	1.717	1.252	3.00	3.63
97	314.909	43.418	11.095	0.896	0.309	2.934	1.838	1.310	3.63	2.82
98	314.910	43.933	11.222	1.071	0.357	2.803	2.373	1.347	4.43	2.86
99	314.911	44.258	11.909	0.835	0.250	2.574	1.581	1.147	2.66	4.34
100	314.912	44.183	10.717	1.112	0.369	2.836	2.096	1.396	4.63	2.24
101	314.916	43.378	10.050	0.795	0.217	2.678	1.678	1.158	2.11	1.90
102	314.923	43.483	10.960	0.703	0.226	2.091	1.303	0.935	2.26	2.86
103	314.924	43.482	12.371	0.801	0.239	2.539	1.597	1.128	2.47	5.42
104	314.926	43.308	8.900	0.764	0.241	2.593	1.643	1.213	2.51	1.09

8. THE OBSERVED $g-r$, $r-i$ DIAGRAM

Figure 7 shows the $g-r$ vs. $r-i$ diagram for the same sample of stars. The sequences of luminosity V and III stars shown in the diagram were taken from Table 1, they correspond to the $g-r$ index combined from two photometric systems, MegaCam and IPHAS, with different zero points. In this diagram we see the same features as in the $u-g$ vs. $r-i$ diagram: the unreddened main sequence of G–K–M dwarfs and the rich sequence of reddened A and F stars on the extension of the intrinsic main sequence of these spectral classes. The upper part of this sequence is overlapped by the sequence of reddened RCGs (red crosses). Above it a broad band of reddened K2–K5 giants is located.

The intrinsic sequences of M-type stars, both of dwarfs and giants, turn sharply to the right since an increase in absorption by TiO bands is strongly blocking the intensity in the r passband, thus causing $g-r$ to decrease and $r-i$ to increase. However, there is some disagreement between the values of the observed and synthetic $g-r$ colors – the synthetic sequence is about 0.1 mag above the observed one. This can be caused by systematic errors either in spectral energy distributions or in the response functions of the passbands. On the other hand, the effect of systematic errors in the observed color indices cannot be excluded.

As in other two-color diagrams, in the $g-r$ vs. $r-i$ diagram the majority of the identified RCGs (red crosses) form a quite distinct strip along their reddening lines. At the same time, a few stars exhibit considerable deviations from the bulk of points on either side of the strip. This means that either their classification as RCGs is wrong or there are other reasons for such deviations (errors in photometry, binarity, metal-deficiency, peculiarity, etc.).

9. THE DEPENDENCE OF EXTINCTION ON DISTANCE

For stars in Table 2 the values of interstellar extinction and distance given in the last two columns (taking $M_{K_s} = -1.6$) were calculated using the following formulae:

$$A_{K_s} = 2.0 E_{H-K_s} = 2.0 [(H - K_s) - 0.09], \quad (6)$$

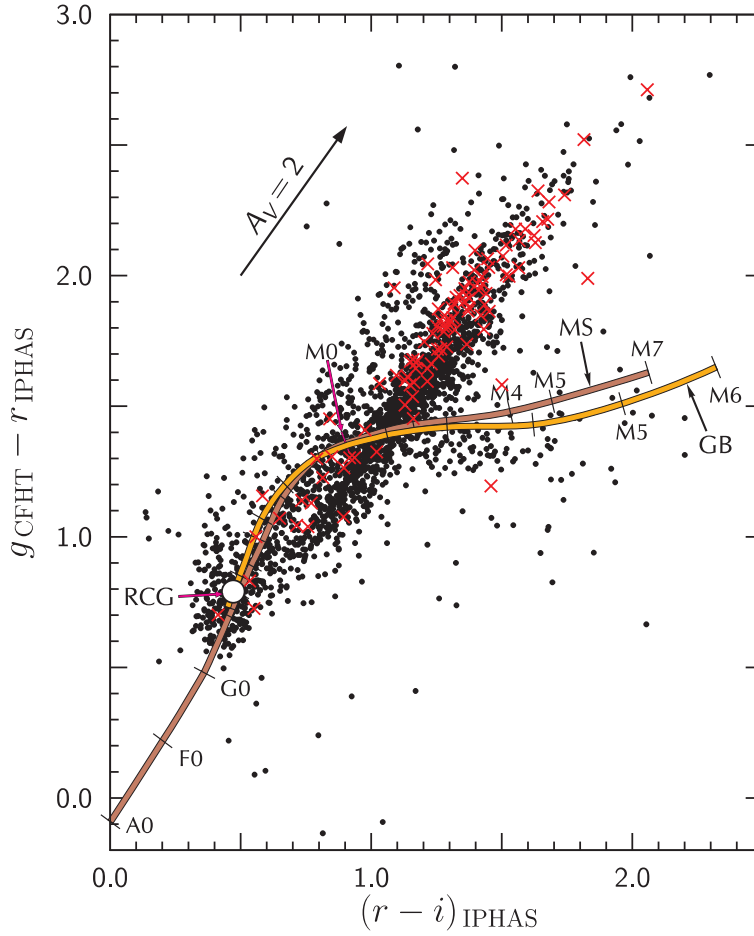


Fig. 7. Observed stars in the $g-r$ vs. $r-i$ diagram. The main sequence and the giant branch from Table 1 are shown. Red crosses denote the suspected RCGs.

$$5 \log d = K_s - M_{K_s} + 5 - A_{K_s}, \quad (7)$$

$$A_V = 8.3 A_{K_s}. \quad (8)$$

In Figure 8 the extinctions A_V are plotted against distance, together with the results obtained in the direction of LDN 935 by Laugalys et al. (2006) from *Vilnius* photometry. The stars with *Vilnius* photometry are plotted as dots, the RCGs from Table 2 in the direction of the dark cloud as open circles and in the direction of the apparently transparent parts of the area as crosses. It is evident that the values of A_V determined for the newly identified RCGs are in good agreement with the results from *Vilnius* photometry, but extend the data to greater distances. The most distant identified RCGs are at $d \approx 5.5$ kpc, i.e., they are located in the Perseus arm. Their u magnitudes are between 20 and 21, K_s magnitudes are ~ 12.5 and the A_V extinctions 2.5–3.5 mag.

It should be noted, however, that the RCGs identified using the MegaCam + IPHAS data are located mostly in relatively transparent directions, so they do not

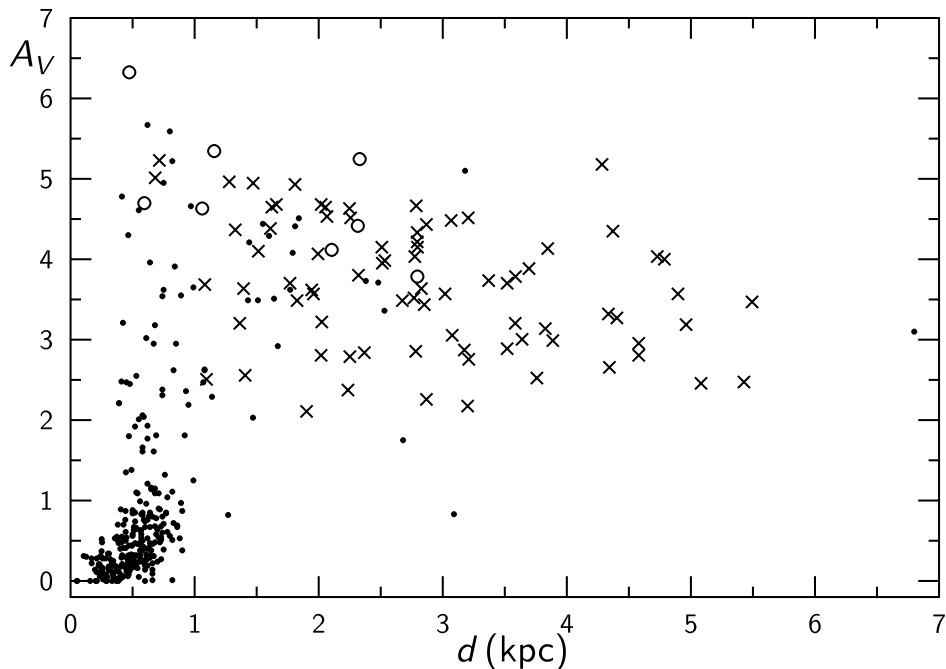


Fig. 8. Interstellar extinction as a function of the distance up to 7 kpc in the NAP complex. Dots denote the data for the dark cloud LDN 935 from Laugalys et al. (2006), open circles denote RCGs in the dark part of the investigated area, and symbols \times denote RCGs in the bright part of the area.

give information about the extinction behind of the dust cloud LDN 935 which covers a large part of the MegaCam area. According to Cambr  sy et al. (2002), the extinction A_V in the densest parts of the cloud can be as large as 35 mag or more. The limiting magnitudes in the MegaCam frames are too small to reach RCGs with $A_V > 6$ mag. However, the extinction values up to 5 mag are met even in the apparently bright areas (for example, in Florida) and at relatively small distances (0.7–2 kpc).

Seventeen stars of Table 2, not plotted in Figure 8, exhibit the values of extinction A_V smaller than 2.0 mag at the 2–6 kpc distances. Other stars at such distances exhibit extinction 2–3 times larger. These stars are probably misclassified as RCGs, they could infiltrate through the above conditions from other sequences due to larger observational errors, peculiarity or duplicity. Six of such stars are projected on the dark cloud and are probably G–K dwarfs or subgiants located in front of the NAP complex. In Table 2 the numbers of these stars are marked with asterisks and their extinctions and distances are not given.

10. DISCUSSION AND CONCLUSIONS

Combining deep photometry obtained in the J , H , K_s system of the 2MASS survey, the u , g system of the MegaCam survey and the r , i system of the IPHAS survey we proposed a method how to isolate a group of stars containing the core He-burning red clump giants with an admixture of shell H-burning giants of spectral

classes G5–K1 and M2–M3. To isolate RCGs the method uses five conditions which enable to reject stars of other types in the diagrams $J-H$ vs. $H-K_s$, $u-g$ vs. $r-i$ and K_s vs. $H-K_s$. Since RCGs are absolutely bright (especially in the near infrared) and have a tight range of absolute magnitudes and colors, they can be used for the investigation of interstellar extinction to large distances.

The method was applied to an area of $1^\circ \times 1^\circ$ in the direction of the North America and Pelican (NAP) nebulae, which covers a considerable part of the dark cloud LDN 935 including the Gulf of Mexico and the ‘coastal’ areas around it. The identified 87 RCGs, listed in Table 2, are to be verified in the future by spectral observations.

For the identified RCGs, the values of interstellar extinction and distances are calculated. The obtained A_V vs. distance relation in the area is in agreement with that found by Laugalys et al. (2006) using the *Vilnius* seven-color system but is extended to larger distances. However, for the isolation of RCGs we need an ultraviolet passband, and this limits the penetration distance. Fainter stars should be measured either with longer exposures or with larger telescopes.

When the ultraviolet magnitudes are not available, we may relax the conditions and isolate RCGs together with an admixture of red giants from a wider range of spectral classes – G5III to M3III. In this case the $J-H$ vs. $H-K_s$ diagram (Figure 2) is sufficient. The isolated star sample will be not uniform in absolute magnitudes, but the difference in the intrinsic $H-K_s$ color indices in this range of spectral classes is only 0.25 mag. At heavy interstellar reddening such a dispersion in color excesses is not critical. Consequently, background stars on the red giant sequence can be used for mapping the interstellar extinction of an isolated cloud if their number is statistically significant. This method should be more accurate than the NICE (Lada et al. 1994) and NICER (Lombardi & Alves 2001) methods which use stars of all spectral types mixed together. The main shortcoming of our method is that it requires a statistically significant number of background giants observed behind the cloud.

ACKNOWLEDGMENTS. The use of the 2MASS, MegaPipe, IPHAS, SkyView, Gator and Simbad databases is acknowledged. This research used the facilities of the Canadian Astronomy Data Centre operated by the National Research Council of Canada with the support of the Canadian Space Agency. We are thankful to Edmundas Meistas, A. G. Davis Philip and Stanislava Bartašiūtė for their help in preparing the paper. Credit for color picture of the North America and Pelican nebulae: Adam Block/NOAO/AURA/NSF.

REFERENCES

- Alves D. R. 2000, ApJ, 539, 732
 Cambrésy L., Beichman C. A., Jarrett T. H., Cutri R. M. 2002, AJ, 123, 2559
 Comerón F., Pasquali A. 2005, A&A, 430, 541
 Corbally C. J., Straižys V., Laugalys V. 2009, Baltic Astronomy, 18, 111 (this issue)
 Covey K. R., Ivezić Ž., Schlegel D. et al. 2007, AJ, 134, 2398
 Dobashi K., Uehara H., Kandori R., Sakurai T., Kaiden M., Umemoto T., Sato F. 2005, PASJ, 57, S1
 Drew J. E., Greimel R., Irwin M. J. et al. 2005, MNRAS, 362, 753

- Grocholski A. J., Sarajedini A. 2002, *AJ*, 123, 1603
- Gwyn S. D. J. 2008, *PASP*, 120, 212
- Lada C. J., Lada E. A., Clemens D. P., Bally J. 1994, *ApJ*, 429, 694
- Laugalys V., Straizys V., Vrba F. J., Boyle R. P., Philip A. G. D., Kazlauskas A. 2006, *Baltic Astronomy*, 15, 483
- Lombardi M., Alves J. 2001, *A&A*, 377, 1023
- Lynds B. T. 1962, *ApJS*, 7, 1
- MegaPipe 2009, <http://www2.cadc-ccda.hia-ihp.nrc-cnrc.gc.ca/megapipe>
- Oke J. B. 1965, *ARA&A*, 3, 23
- Perryman M. A. C., Lindegren L., Kovalevsky J. et al. 1995, *A&A*, 304, 69
- Perryman M. A. C., Lindegren L., Kovalevsky J. et al. 1997, *A&A*, 323, L49
- Straizys V. 1992, *Multicolor Stellar Photometry*, Pachart Publishing House, Tucson, Arizona; available in electronic form from the author
- Straizys V., Laugalys V. 2007, *Baltic Astronomy*, 16, 327
- Straizys V., Laugalys V. 2008a, *Baltic Astronomy*, 17, 1
- Straizys V., Laugalys V. 2008b, *Baltic Astronomy*, 17, 143
- Straizys V., Laugalys V. 2008c, *Baltic Astronomy*, 17, 253
- Straizys V., Corbally C. J., Laugalys V. 2008, *Baltic Astronomy*, 17, 125
- Straizys V., Lazauskaitė R. 2009, *Baltic Astronomy*, 18, 19
- Sviderskienė Z. 1988, *Bull. Vilnius Obs.*, No. 80, 3
- Sviderskienė Z. 1992, *Bull. Vilnius Obs.*, No. 86, 3